AGU PUBLICATIONS

JGR

Journal of Geophysical Research: Atmospheres

RESEARCH ARTICLE
10.1002/2017JD026942

Key Points:
- Downslope winds resulted in strong low-level vertical wind shear, which interacted with the development of near-surface positively buoyant air during the morning and generated significant turbulence kinetic energy
- The strong and gusty winds caused moderate meso-γ- to β-scale dust storms as an early stage of precursor to later severe dust storms that affected large areas

Correspondence to:
A. K. Pokharel,
ashokpokharel@hotmail.com

Citation:
Pokharel, A. K., Kaplan, M. L., & Fiedler, S. (2017). Subtropical dust storms and downslope wind events. *Journal of Geophysical Research: Atmospheres, 122*, 10,191–10,205. https://doi.org/10.1002/2017JD026942

Received 23 APR 2017
Accepted 9 SEP 2017
Accepted article online 14 SEP 2017
Published online 6 OCT 2017

Subtropical Dust Storms and Downslope Wind Events

Ashok Kumar Pokharel[1,2], Michael L. Kaplan[2], and Stephanie Fiedler[3]

[1]Department of Atmospheric Sciences, University of Nevada, Reno, NV, USA, [2]Division of Atmospheric Sciences/Desert Research Institute, Reno, NV, USA, [3]Max-Planck-Institute for Meteorology, Hamburg, Germany

Abstract We performed detailed mesoscale observational analyses and Weather Research and Forecasting (WRF) model simulations to study the terrain-induced downslope winds that generated dust-emitting winds at the beginning of three strong subtropical dust storms in three distinctly different regions of North Africa and the Arabian Peninsula. We revisit the Harmattan dust storm of 2 March 2004, the Saudi dust storm of 9 March 2009, and the Bodélé Depression dust storm of 8 December 2011 and use high-resolution WRF modeling to assess the dynamical processes during the onset of the storms in more depth. Our results highlight the generation of terrain-induced downslope winds in response to the transition of the atmospheric flow from a subcritical to supercritical state in all three cases. These events precede the unbalanced adjustment processes in the lee of the mountain ranges that produced larger-scale dust aerosol mobilization and transport. We see that only the higher-resolution data sets can resolve the mesoscale processes, which are mainly responsible for creating strong low-level terrain-induced downslope winds leading to the initial dust storms.

1. Introduction

The Sahara, which lies in North Africa, represents a major subtropical desert that spans approximately 5600 km from the Atlantic coast to the shores of the Red Sea. This region represents the most prolific aeolian dust source on our planet (Prospero et al., 2002; Washington et al., 2003), where a variety of different dust storm occur. Ozer (2001) found that the maximum frequency of dust storms over West Africa occurs from local 9:00 h to 15:00 h due to the enhancement of dry convection in the planetary boundary layer during the day and minimum frequency at night between local 21:00 h and 3:00 h. More recent studies on the role of convective cold pools and nocturnal low-level jets indicate that roughly half of the summerime dust emission is attributed to these processes (Heinold et al., 2013). In winter and spring, Harmattan surges have been identified to be particularly important for generating dust storms, when synoptic-scale cold air advection occurs over North Africa (Fiedler, Kaplan, & Knippertz, 2015). Harmattan winds can transport a significant amount of mineral dust equatorward across inhabited regions in sub-Saharan Africa where the dust causes severe weather conditions with adverse impacts on visibility, agriculture, and human health (Burton et al., 2013; Kalu, 1979).

The Bodélé Depression occupies only an area of 0.2% of the Sahara, located northeast of Lake Chad, but is the most active dust source region in the world (Koren et al., 2006). The Tibesti Mountains to the north and the Ennedi Mountains in the east of the Bodélé Depression form a large hollow valley (Koren & Kaufman, 2004). The Bodélé Depression has ideal prerequisites for dust emission due to the hyperaridity (annual average rainfall $<$10 mm) (New et al., 2002), the absence of vegetation, and fine sediments prone to wind erosion. Strong surface winds over the Bodélé Depression are suitable conditions for the occurrence of dust storms (Todd et al., 2007; Washington & Todd, 2005). Here downslope winds and gap winds are believed to form a favorable environment for generating dust-emitting peak winds, often associated with the formation of nocturnal low-level jets (Fiedler et al., 2013; Schepanski et al., 2009; Washington & Todd, 2005).

The Middle East is another major dust-affected region. Dust storms occur here primarily during the months of May to August on the Arabian Peninsula (Barkan, Kutiel, & Alpert, 2004; Washington et al., 2003) when there is intense solar radiation and high wind speeds. The early dust storm of 9 March 2009 was not predicted and caused severe impacts, such as respiratory problems of people in the northeastern, eastern, and central parts of Saudi Arabia and most of Kuwait (Alharbi, Maghrabi, & Tapper, 2013). This storm, which lasted several hours and struck Riyadh, was one of the most intense dust storms experienced in Saudi Arabia over the last two decades. The event was characterized by an increase of the surface relative humidity by 33%, a reduction of the temperature by 6°K, and nearly nonexistent visibility of just 1 m for some time (Maghrabi et al., 2011).

In a previous study of the role of jet streak dynamics on dust storm genesis, Pokharel, Kaplan, and Fiedler (2016) determined that a major North African dust storm was preceded by a weaker event in northwest Africa in the lee of the Atlas Mountains. The findings pointed to a terrain-induced downslope wind as a possible reason for these small-scale and more isolated precursor peak wind events, before the occurrence of the major large-scale events that was associated with strong baroclinic jet streak adjustments.

Here we pursue the evaluation of the role of terrain-induced wind storms during that event in more detail and expand the analysis of similar dust storms in another two regions adjacent to mountain ranges. We choose three case studies of dust storms, namely, (1) the Harmattan dust storm of 2 March 2004 in North Africa, (2) the Saudi dust storm of 9 March 2009, and (3) a severe Bodélé Depression dust storm of 8 December 2011.We aim to reveal commonalities and differences of the terrain-induced peak wind events, which were responsible for dust emission just before the onset of the three large-scale dust storms that occurred in North Africa and the Arabian Peninsula. We are particularly interested in such small-scale structures of the events because these small-scale downslope winds are precursors that help precondition the environment for larger-scale events by ablating dust and lifting it into the boundary layer, so the subsequent larger-magnitude turbulence kinetic energy (TKE) events are better able to transport the dust.

The next section reviews the literature on the theoretical background of downslope wind events. Section 2 describes our methodology, section 3 discusses the results and discussion, and section 4 presents a conclusion of the key findings.

1.1. Relevant Theories of Downslope Wind Formation

The literature on downslope wind formation is very extensive; thus, we will only focus on the key theories. Early on, three theories of windstorm formation on the leeside of mountain ranges are employed frequently. First, shallow water theory indicates that a transition from subcritical to supercritical flow upstream of a mountain range leads to an accelerating cross-mountain flow and an hydraulic jump accompanied by strong winds in the lee (e.g., Durran, 1990; Houghton & Kashara, 1968; Smith, 1985). Klemp and Lilly (1975) formulated a linear mountain wave theory, which can be applied under less restrictive conditions than the concept of a hydraulic jump. Their theory attributes the generation of leeside peak winds to the tuning of the wave phase in the middle upper troposphere and in levels below the mountaintop. Peltier and Clark (1979) first employed nonlinear theory to determine that wave breaking accompanying a self-induced wave critical level led to extreme wind events. The critical level for self-induced wave breaking strongly depends on the strength of the temperature inversion and the vertical wind shear.

In contemporary literature we see these three reorganized such that earlier hydraulic theories, which are based on homogeneous fluid flow (basically shallow water system), can be synthesized under Smith's (1985) nonlinear hydraulic theory with stratified fluid flow. Smith's (1985) theory is completely different from the resonant amplification theory proposed by Peltier and Clark (1979). It is to be noted that Smith's hydraulic theory includes a development of hydraulic jump embedded in a dead region occupied by highly turbulent flow enclosed by divided streamlines. Both of these broader categories of theories rely on a strong low mid-level inversion and transition to accelerating flow from the windward to lee of the mountain, thus creating the need for discontinuous stratification and strong winds aloft.

2. Materials and Methods

We first use satellite imagery to characterize dust events. These include a composite of the Moderate Resolution Imaging Spectroradiometer (MODIS)/Aqua and Terra (level 1b, collection 51, 1 km horizontal resolution, and RGB composite) (https://ladsweb.nascom.nasa.gov) (Figure 1), Meteosat-8 from the European Organization for the Exploitation of Meteorological Satellites (http://www.eumetsat.int/website/home/Images/ImageLibrary/DAT_IL_04_03_06_F.html), and aerosol optical depth derived from the MODIS/Aqua instrument level 3 daily (D3). Rawinsonde soundings were obtained from the University of Wyoming, and observational surface data from Weather Underground, listed in Table 1. The coarse-scale evolution of the dust storms are studied with an aerosol-weather model simulation of $1° \times 1°$ horizontal resolution from the Navy Aerosol Analysis and Prediction System (NAAPS) (https://www.nrlmry.navy.mil/aerosol_web/). This model displays dust predictions at 6 h intervals, which will also be used to diagnose the beginning and subsequent multiple occurrences of dust storms over our region of interest. The NAAPS product is derived from a

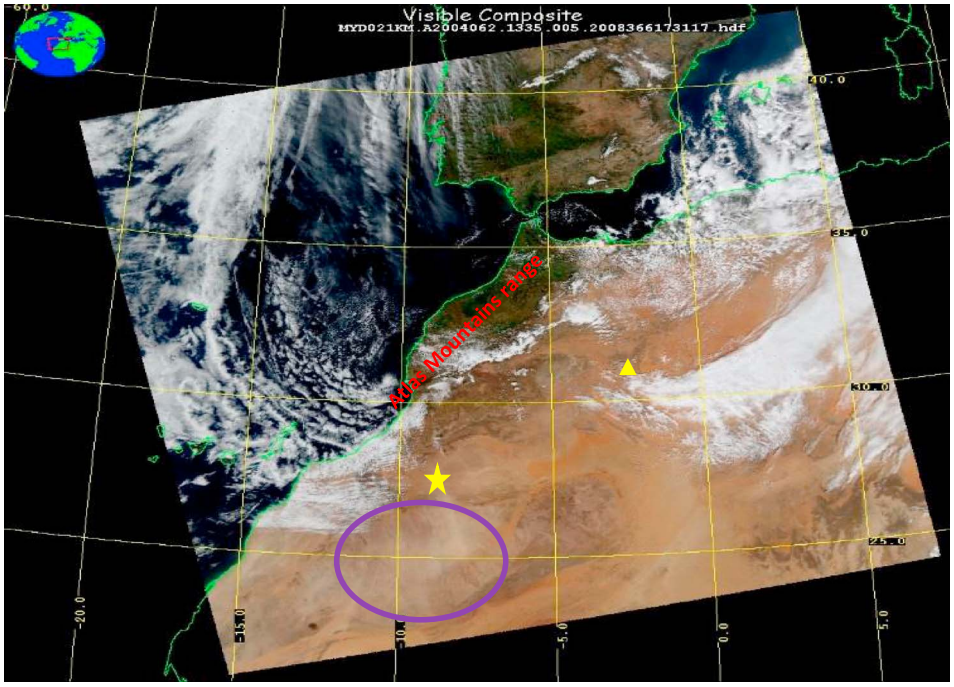

Figure 1. Dust storm image captured by MODIS/Aqua at 1335 UTC on 2 March 2004 (source: https://ladsweb.nascom.nasa.gov). Yellow star indicates the surface observational station at Tindouf (*x* and *y* coordinates of Tindouf are mentioned in section 2) in Algeria, which experienced the dust storm in the early parts of 2 March 2004 (source: wunderground.com). Yellow triangle indicates sounding station at Bechar in Algeria. The purple colored circle shows the area of dust plume.

very sophisticated ensemble-driven system, for example, the Ensemble of the Navy Aerosol Analysis Prediction System (ENAAPS). The system makes use of an ensemble of the ENAAPS combined with an ensemble adjustment Kalman filter from the National Center for Atmospheric Research's (NCAR) Data Assimilation Research Testbed (Rubin et al., 2016). In addition to this, the Modern-Era Retrospective Analysis for Research and Applications-2 (MERRA-2) model (spatial resolution 0.5 × 0.625°) hourly data sets were used to analyze the dust scattering aerosol optical thickness (AOT) 550 nm of 1 μm particulate matter over this region of interest (https://giovanni.gsfc.nasa.gov/giovanni/). For in-depth synoptic-scale to mesoscale observational atmospheric processes, the reanalysis data set of surface pressure, geopotential height, air temperature, wind speed and direction, vertical motion, vertically integrated atmospheric mass tendency, and kinetic energy due to pressure gradient force obtained from the Modern-Era Retrospective Analysis for Research and Applications (MERRA) (https://disc.sci.gsfc.nasa.gov/mdisc/data-holdings/merra/merra_products_nonjs.shtml; Rinecker et al., 2011) were analyzed. These data were used to make horizontal cross sections at different pressure levels as well as vertical cross sections of *u*-wind speed, *v*-wind speed components, and potential temperature at a resolution of 0.50° × 0.67°.

To achieve finer temporal and spatial resolution of the atmospheric processes involved in the dust storms, experiments with the nonhydrostatic Weather Research and Forecasting (WRF) model (Skamarock et al., 2008)

Table 1
Observational Surface Archived by Weather Underground and the Available Stations

Dust storm case	Surface stations where the dust storms were observed	Date	Time (UTC)	Wind direction	Wind speed (m/s)	Visibility (km)
Harmattan dust storm case	Tindouf	2 March 2004	0900–1200	Northwesterly/west-northwesterly	16.4–18.5	1.9–6.9
Saudi dust storm case	Arar	9 March 2009	0900	North-northwesterly	7.19	6.4
	Hafr-Al-Batin	9 March 2009	0900	Southwesterly	8.22	6.4
	Madinah	9 March 2009	0900	West-southwesterly	2.6	5.6
Bodélé dust storm case	Ndjamena	8 December 2011	0600	Northeasterly	3	5.95

Table 2
Horizontal Grid Dimensions and Integration Times in WRF Simulation of All Three Dust Storm Cases

Dust storm cases	Horizontal grid dimensions (west-east and north-south directions)	Integrated time
Harmattan dust storm	82 × 118 grid points (54 km grid spacing)	1200 UTC 1 March to 0600 UTC 3 March 2004
	208 × 274 grid points (18 km grid spacing)	1200 UTC 1 March to 0600 UTC 3 March 2004
	502 × 613 grid points (6 km grid spacing)	1200 UTC 1 March to 0600 UTC 3 March 2004
	802 × 802 grid points (2 km grid spacing)	1200 UTC 2 March to 0600 UTC 3 March 2004
Saudi dust storm	82 × 97 grid points (54 km grid spacing)	1200 UTC 8 March to 0000 UTC 10 March 2009
	208 × 232 grid points (18 km grid spacing)	1200 UTC 8 March to 0000 UTC 10 March 2009
	502 × 553 grid points (6 km grid spacing)	0600 UTC 9 March to 0000 UTC 10 March 2009
	802 × 760 grid points (2 km grid spacing)	1200 UTC 9 March to 0000 UTC 10 March 2009
Bodélé dust storm	82 × 97 grid points (54 km grid spacing)	0000 UTC 8 December to 0600 UTC 9 December 2011
	208 × 232 grid points (18 km grid spacing)	0000 UTC 8 December to 0600 UTC 9 December 2011
	502 × 553 grid points (6 km grid spacing)	0000 UTC 8 December to 0600 UTC 9 December 2011
	802 × 760 grid points (2 km grid spacing)	0600 UTC 8 December to 0600 UTC 9 December 2011

were performed for each storm, listed in Table 2. We used four nested domains with horizontal resolutions of 54, 18, 6, and 2 km, of which resolutions higher than 18 km were run without allowing moist convection to be turned in as a parameterization as convection was virtually nonexistent in these case studies. The lateral boundary data of the parent domain with the coarsest resolution were obtained from the National Center for Environmental Prediction/Global Forecasting System (1° × 1°) products. For instance for the Harmattan case, the WRF model was initialized over a parent domain with a horizontal grid of 82 × 118 grid points of 54 km horizontal grid spacing in the west-east and north-south directions. Three domains were than nested into the parent domain at 18, 6, and 2 km. The locations of the simulation domains for the three cases are depicted in Figures 2, 8, and 12.

The WRF simulations used the following physical parameterizations: (i) momentum and heat fluxes at the surface (Janjić, 1996, 2001) following Monin-Obukhov similarity theory, (ii) turbulent mixing following the Mellor-Yamada-Janjić 1.5 order (level 2.5) turbulence closure model (Janjić, 2001; Mellor & Yamada, 1974), (iii) moist convection following the Betts-Miller-Janjić cumulus scheme (Betts, 1986; Betts & Miller, 1986; Janjic, 1994) for the simulations with 54 and 18 km horizontal resolution, (iv) cloud microphysical processes following the Thompson double-moment scheme (Thompson et al., 2006; Thompson, Rasmussen, & Manning, 2004), (v) radiative processes following the rapid radiative transfer model for longwave radiation (Mlawer et al., 1997) and Dudhia's scheme for shortwave radiation (Dudhia, 1989), and (vi) land-surface processes from the Noah land surface model (Chen & Dudhia, 2001; Ek et al., 2003).

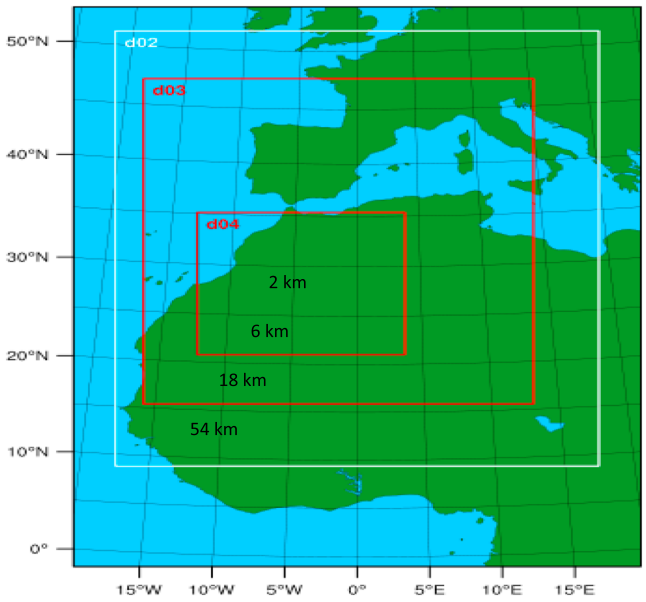

Figure 2. WRF domain configuration for the Harmattan dust storm case in Figure 1 (Pokharel, 2016). do1, do2, do3, and do4 represent domains of 54, 18, 6, and 2 km resolution, respectively.

3. Results and Discussion

3.1. Harmattan Dust Storm Case Study

3.1.1. Joint Observational and Model Analyses

The vertical temperature and wind profiles at different pressure levels close to the time period of the early dust storm are shown by the rawinsonde soundings at Bechar in Algeria (31.50°N, 2.25°W) for 2 March 2004 at 0000 UTC in Figure 3a. Bechar lies in the lee and close to the Atlas Mountains, so that we expect that the observations here are representative for the location where downslope peak winds occur. The sounding at 0000 UTC on 2 March showed a shallow inversion between 925 and 900 hPa and a dry adiabatic lapse rate between 900 and 600 hPa (Figure 3a). The sounding indicates a warm low-level layer under an adiabatic layer aloft that can be an elevated residual well-mixed layer (EML) that had formed in the previous day above the nearby mountains. With westerly winds above the mountain the EML was likely advected downstream toward Bechar. Above this

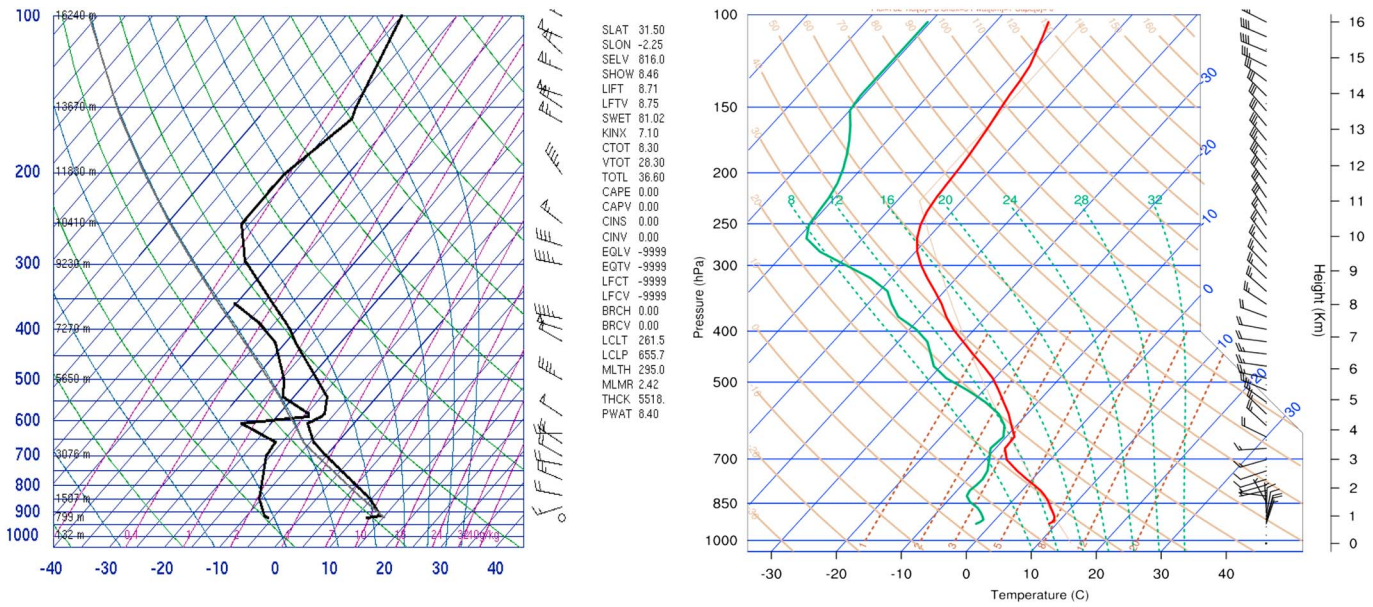

Figure 3. (a) Atmospheric soundings at 0000 UTC 2 March 2004 at Bechar in Algeria (source: University of Wyoming). (b) Atmospheric soundings at 0000 UTC 2 March 2004 at Bechar in Algeria plotted from WRF simulation (6 km resolution).

deep dry adiabatic layer, there was again a shallow inversion layer around 600 hPa. Hence, Figure 3a shows that there were multiple stratified layers (such as the inversion layer at the surface, presence of the deep dry adiabatic lapse rate above that inversion, and a thin inversion layer above that deep dry adiabatic layer), which indicate the presence of the discontinuous stratification of the atmosphere over this area at that time. This is also shown by the soundings of WRF simulation of 6 km resolution (Figure 3b)—an indication of the validation of the WRF model. This complex stratification shown by the Figures 3a and 3b on the lee of the Atlas Mountains infers the possible disruption of the cross-mountain flow by the barrier consistent with differential sinking and stable stratified layers, for example, possibly blocking the flow. In order to diagnose the response of the airflow over the mountains finer scale analysis with a higher-resolution data set is required.

Surface observations at Tindouf (27.67°N, 8.13°W; Figure 1) in Algeria report a dust storm at 0900 UTC on 2 March 2004. This dust storm was associated with northwesterly and west northwesterly winds, which ranged from 16.4 to 18.5 ms^{-1} (Table 1). During this period the wind speed and visibility were negatively correlated at this station and the visibility was reduced to 1.93 km due to blowing dust. This is likely not solely a local event, since the NAAPS dust concentration product shows large surface dust concentrations over the southwest, central, and eastern regions of Algeria during the morning of 2 March. Beginning at 0000 UTC 2 March 2004 the strength and the areal extension of the surface dust concentration continuously increased from 1280 to 5120 $\mu g/m^3$, particularly over the northeast region of Algeria. The MERRA-2 model shows that the dust scattering AOT ranged from 0.067 to 0.25 over this region. The most substantial dust emission events are associated with unbalanced jet streak adjustment processes, discussed in depth in Pokharel (2016) and Pokharel, Kaplan, and Fiedler (2016). Here we briefly revisit the synoptic situation to put the preceding conditions that are the focus of this study into a wider context. The midtropospheric synoptic overview from the MERRA indicates that, during the early period of 2 March 2004, there was a positively tilted trough over the region of interest. The trough was characterized by ageostrophic winds indicative of the development of curved flow by the change of the wind direction (e.g., initiation of rotation/cyclonic curvature vorticity) near the trough axis at 28°N, 1°W–32°N, 3°E. The positively tilted trough strengthened in curvature further till the occurrence of widespread and intense dust emission. The associated temporal development of the geopotential height, namely, the deep cold positively tilted trough with falling heights, acts as an upper air disturbance over the Djeifa, Laughout, Bechar, and Taghit of Algeria (north to west part of Algeria). The preceding cross-mountain flow is analyzed in more detail.

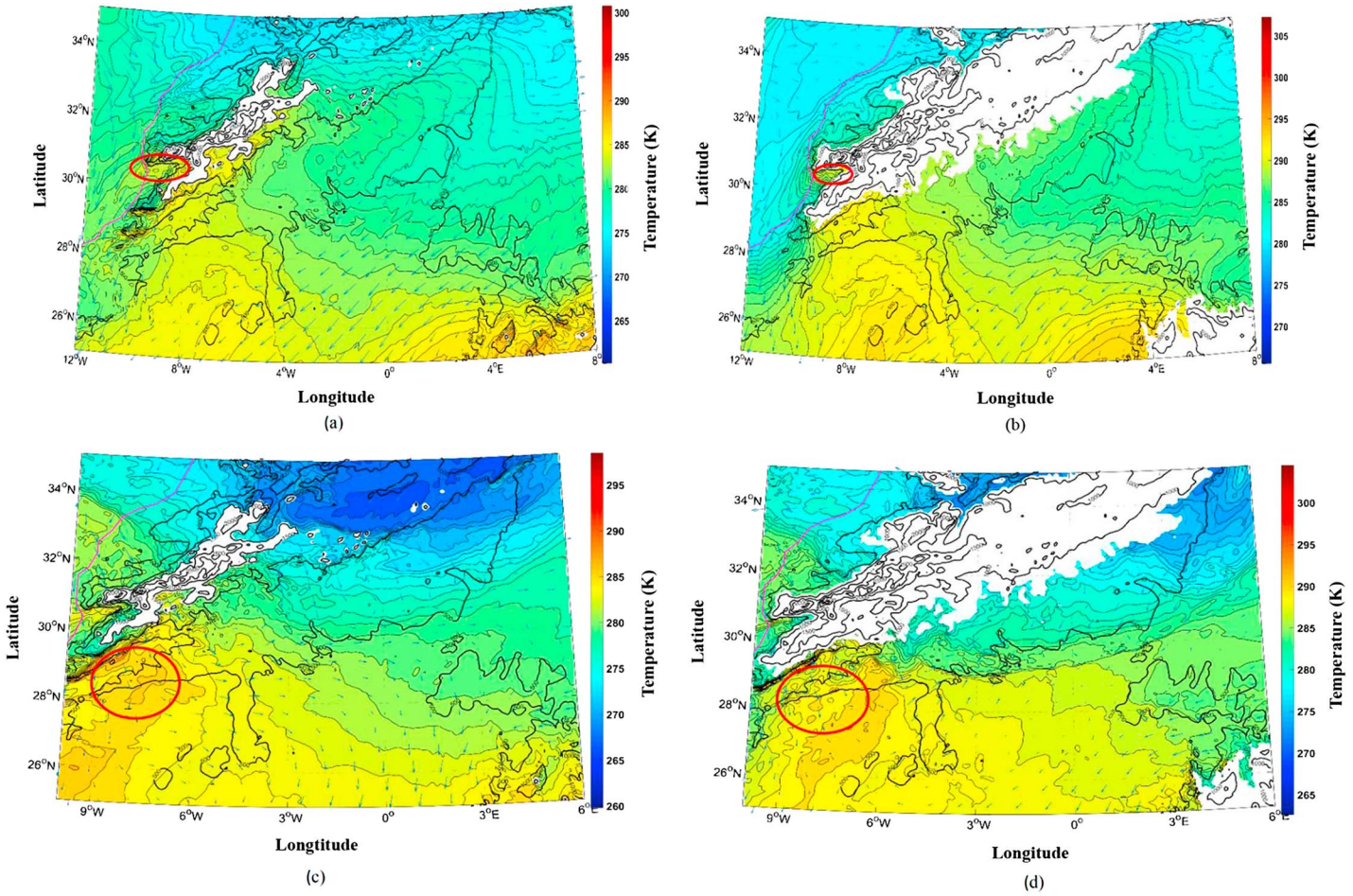

Figure 4. (a) Temperature (shaded) and wind (vector) at 850 hPa at 1500 UTC on 1 March 2004 from the high resolution (6 km). The circled area marks the warming region on the windward side of the Atlas Mountains. The black contours mark the orographic height in increments of 500 m. (b) Temperature (shaded) and wind (vector) at 925 hPa at 1500 UTC on 1 March 2004 from the high resolution (6 km). The black contours mark the orographic height in increments of 500 m. The circled area marks the warming region on the windward side of the Atlas Mountains. (c) Temperature (shaded) and wind (vector) at 850 hPa at 0600 UTC on 2 March 2004 from the high resolution (6 km). The black contours mark the orographic height in increments of 500 m. (d) Temperature (shaded) and wind (vector) at 925 hPa at 0600 UTC on 2 March 2004 from the high resolution (6 km). The black contours mark the orographic height in increments of 500 m.

3.1.2. WRF Simulation Analyses

There was the presence of the well-mixed/warm layer from the surface to the lower tropospheric in the upstream of the Atlas Mountains in the afternoon (1500 UTC) of 1 March 2004 which is shown from the horizontal cross sections of 850 hPa and 925 hPa of wind speed/direction and temperature (plots of WRF-simulated output of 6 km grid spacing) in Figures 4a and 4b. On the early part of 2 March the air adjacent to the bottom of the lee slope of the south/southwestern edge of the Atlas Mountains was quite warm. This warm layer was indicative of the possibility of a significant downslope wind near the surface and the advection of the residual well-mixed and elevated convective planetary boundary layer from the previous afternoon, which formed above the Atlas Mountains. This EML was confirmed from observed soundings (Figure 3a) and the WRF simulated horizontal cross sections of 850 hPa and 925 hPa wind speed/direction and temperature (plots of WRF-simulated output of 6 km grid spacing) over the 27–29°N, 7–10°W at 0000–0600 UTC on 2 March (Figures 4c and 4d). This simulated downslope compressed layer had a deep dry adiabatic lapse rate in the early morning hours on 2 March consistent with the sounding data at Bechar (Figure 3a), and this lapse rate is consistent with overturning isentropes of the WRF simulation. With surface heating during the early morning solar cycle there was an increase in the convective turbulence even with relatively weak wind conditions which facilitated the generation of the dust from the surface at 0600 UTC of 2 March over the ~28–29°N, 9.12°W region as also shown in a case study in Klose and Shao (2013). This

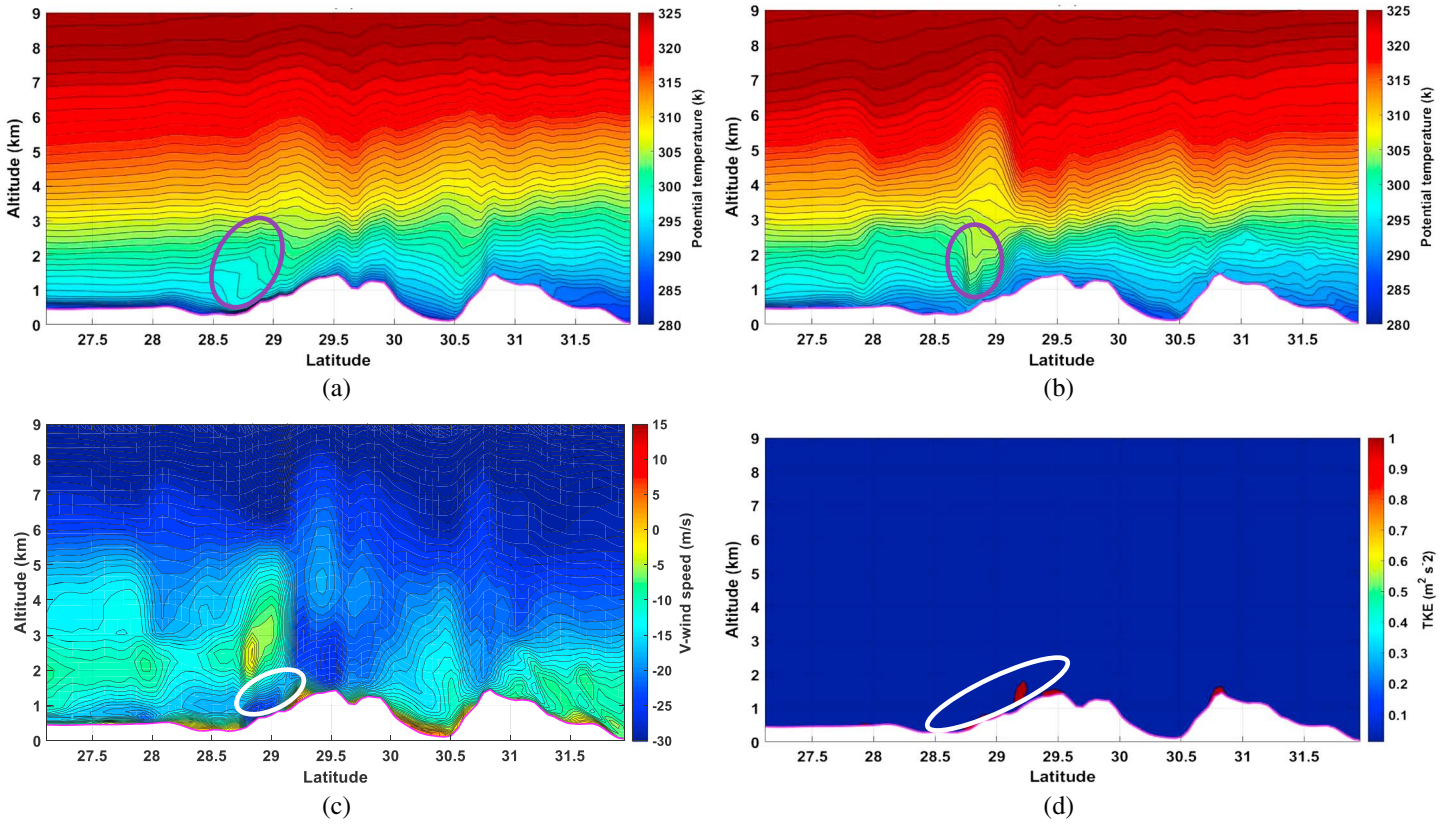

Figure 5. (a) Vertical cross sections of potential temperature (shaded) at 9.12°W at 0000 UTC on 2 March 2004 (6 km resolution WRF product). The blue circled area marks the blocking of the flow. (b) Vertical cross sections of potential temperature (shaded) at 9.12°W at 0900 UTC on 2 March 2004 (6 km resolution WRF product). The blue circled area marks the downslope winds. (c) Vertical cross sections of *v*-wind speed (shaded) at 9.12°W at 0900 UTC on 2 March 2004 (6 km resolution WRF product). Positive and negative magnitudes of *v*-wind components indicate southerly and northerly winds, respectively. The white circled area marks the strong wind shear. (d) Vertical cross sections of turbulence kinetic energy (TKE) at 9.12°W at 0900 UTC on 2 March 2004 (6 km resolution WRF product). The white circled area marks the TKE.

wind maximum can be further substantiated based on the surface dust concentration evolution at this time in the NAAPS plot.

To confirm the downslope wind flow as expected in the sounding at Bechar, vertical cross sections of the isentropic surfaces at 0000 UTC of 2 March were plotted from the 6 km grid spacing WRF simulation output near Tindouf (Figure 5a), where the dust storm was recorded in the observations from Weather Underground. Figure 5a shows that at 0000 UTC on 2 March there was a bulging of isentropic surfaces at upper levels (above the mountains) on the windward side of the mountains and the perturbations of *v*-wind speed components at 28.50–29.10°N, 9.12°W (cross sections across north-south directions). Similarly, the upstream Froude number defined for the discontinuous stratification of the air column as stated by Smolarkiewicz and Rotunno (1989),

$$\mathrm{Fr} = \frac{V}{NH} \tag{1}$$

where V is the flow speed, N is the Brunt-Väisälä frequency, and H is the height of the mountain, was 0.63 at 29°N, 9.12°W at 0000 UTC of 2 March (Figure 5a). Over time the magnitude of the Froude number increased to 1.05 at 0900 UTC and afterward, indicative of the transition from subcriticality toward supercriticality resulting in accelerating downslope wind flow in the lee of the Atlas Mountains (Figure 5b). This downslope wind maximum is shown by the sinking and overturning of isentropic surfaces sharply at that location (Figure 5b). Figures 5a and 5b infer that at the beginning the prevailing wind was blocked by the mountains upstream at 0000 UTC due to insufficient kinetic energy to cross the mountains. Over time (at 0900 UTC and afterward) when the kinetic energy of the air parcels became higher than the potential energy of the air parcels, air accelerated as downslope winds in the lee of the mountains. This downslope wind accelerated in the layer

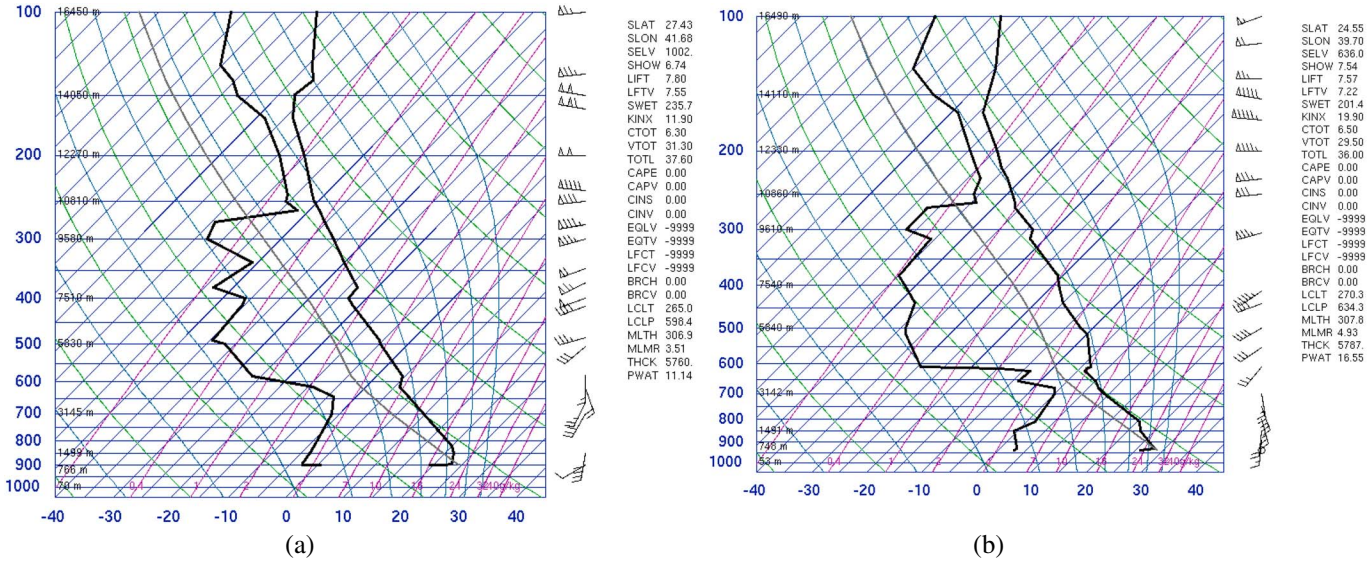

Figure 6. (a) Atmospheric soundings over Ha'il in Saudi Arabia at 0000 UTC on 9 March 2009 (source: University of Wyoming). (b) Atmospheric soundings over Al-Madinah in Saudi Arabia at 0000 UTC on 9 March 2009 (source: University of Wyoming).

between the Atlas Mountains and the overlying inversion as shown, in part, in the simulated sounding as the pressure dropped in the lee of the mountains. Once this wind reached the surface of the lee of the mountains there was a rapid increase in the emission of the dust after the generation of the significant amount of turbulent eddies generated by the contribution of the strong wind shear and the buoyancy (Figures 5c and 5d) source terms in the turbulence kinetic energy (TKE) time tendency equation mentioned by Stull (2000), which is

$$\frac{\partial \mathrm{TKE}}{\partial \mathrm{t}} = -\mathrm{V}.\nabla\mathrm{TKE} + \mathrm{u}*^2\left(\frac{\partial \mathrm{u}}{\partial \mathrm{z}}\right) + \mathrm{g}\left(\frac{\mathrm{Qs}}{Tv}\right) - \varepsilon \tag{2}$$

where $-\mathrm{V}.\nabla\mathrm{TKE}$ is the TKE advection by the mean wind, u_*^2 $(\partial u/\partial z)$ is the generated shear, g $(Qs/T\upsilon)$ define the buoyancy, and ε is the dissipation of TKE or eddy dissipation rate. This is consistent with the direction of the northwesterly/west-northwesterly wind flow during the occurrence of this dust storm observed at Tindouf during 0900–1200 UTC by Weather Underground and the image shown by the MODIS/Aqua at 1335 UTC on 2 March 2004 (Figure 1).

3.2. Saudi Dust Storm Case Study

3.2.1. Joint Observational and Model Analyses

Soundings from the Ha'il (27.43°N, 41.68°E) and Al-Madinah (24.55°N, 39.70°E) rawinsonde stations in Saudi Arabia were used for the analysis of vertical profiles of wind speed/direction and temperature prior to the dust storm (Figures 6a and 6b). The Sarawat Mountains extend along the western border of Saudi Arabia, and these two sounding stations are situated in the lee of the Sarawat Mountains. Thus, it is likely that information regarding the vertical profiles of temperature and wind speed/direction before and after the interaction of the jet stream with the Sarawat Mountains could be depicted by these data for this Saudi case study. At 0000 UTC 9 March soundings from Al-Madinah and Ha'il show a shallow inversion between 940–925 hPa and at 900 hPa (Figures 6a and 6b), respectively. Between 925–625 hPa and 900–625 hPa dry adiabatic lapse rates were present over Al-Madinah and Ha'il, respectively. Above these dry adiabatic layers, shallow stable thermal ridges were present over these regions during that time. This information from two atmospheric soundings shows mutual consistency concerning a shallow inversion at the higher pressure levels (940–900 hPa), a dry adiabatic lapse rate above these higher pressure levels to 625 hPa, and stable thermal ridges above these dry adiabatic lapse rates layers that are similar to the case in northwest Africa. These soundings also indicate important atmospheric features in place before they were taken. For instance, the warm layer at low levels under the cold pool aloft points again to an EML boundary layer that developed during the previous afternoon above the Sarawat Mountains and was subsequently

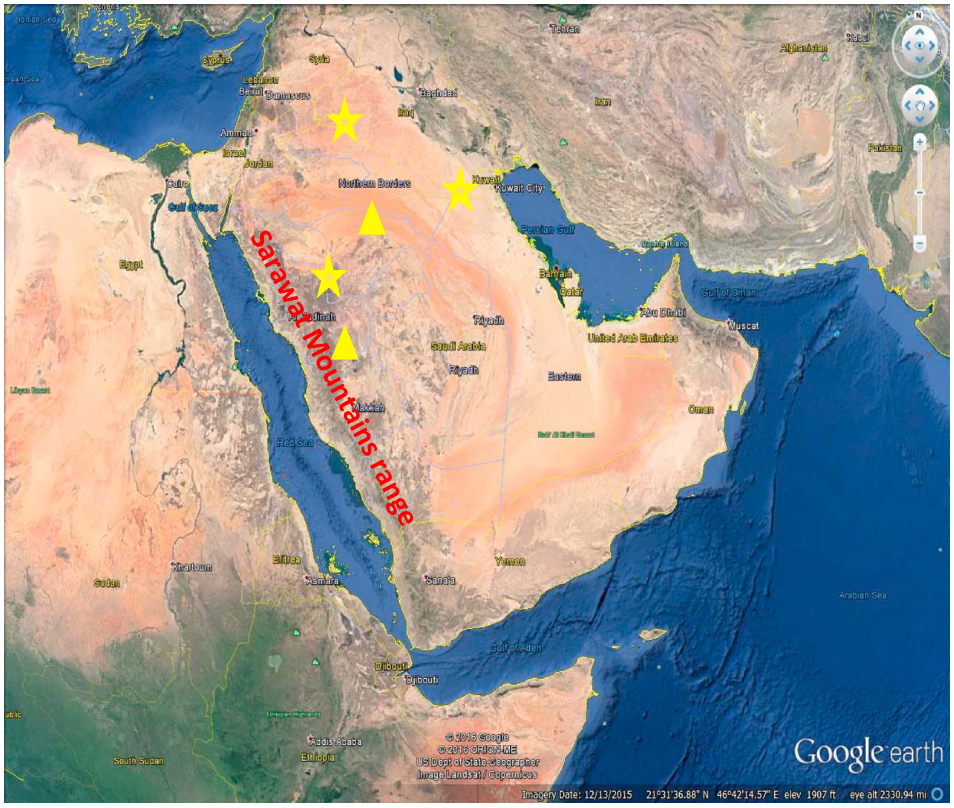

Figure 7. Surface observation stations Arar (30.91°N, 41.14°E), Hafr-Al-Batin (28.32°N, 46.13°E), and Madinah (24.55°N, 39.71°E) in Saudi Arabia are all leeside locations (shown by yellow star), where dust storms were observed in the early period of 9 March (source: wunderground.com). Yellow triangles indicate sounding stations at Ha'il and Al-Madinah in Saudi Arabia.

advected downstream. Due to the influence of the southwesterly winds above the mountain that EML (i.e., the remaining upper mixed layer after the sunset) was likely advected to the Al-Madinah and Ha'il. Above this deep dry adiabatic layer at each of these stations, there was the presence of the shallow inversion layer, which was a warm stable thermal ridge. These different kinds of vertical temperature profiles indicate the presence of discontinuous stratification of the atmosphere at each of these stations at that time. This raises the possibility of the terrain-induced downslope wind flow responsible for causing the dust storm in the lee of the Sarawat Mountains on the early period of 9 March 2009.

Surface observational data archived by Weather Underground show that there was substantially reduced visibility and a dust storm during the early period of 9 March 2009. Arar (30.91°N, 41.14°E), Hafr-Al-Batin (28.32°N, 46.13°E), and Madinah (24.55°N, 39.71°E) are all leeside locations where dust storms were observed in the early period of 9 March (Figure 7 and Table 1).

The NAAPS aerosol model shows that at 0600 UTC of 9 March there were three dust storms based on surface dust concentration increases (500 to 5000 $\mu g/m^3$) aligned over the west (16–25°N, 30–35°E), north/northeast (21–39°N, 38–45°E), and far northeast (39–42°N, 52–58°E) regions of Saudi Arabia, indicating that there were dust storms from 0000 UTC on 9 March onward over Saudi Arabia and its neighboring regions. The dust-scattering AOT over these aforesaid regions were ranging from 0.06 to 0.45 shown by the MERRA-2.

The midtropospheric synoptic overview from the MERRA data sets shows that there was a presence of a negatively tilted trough (northwest to southeast oriented axis) and the development of ageostrophic wind flow consistent with the initiation of the cyclonic thermal vorticity near the trough axis at 28–29N°, 39–41°E due to ageostrophic cold air advection on 9 March. The negatively tilted trough further deepened up to the time of the occurrence of the dust storm. This falling geopotential height is consistent with a

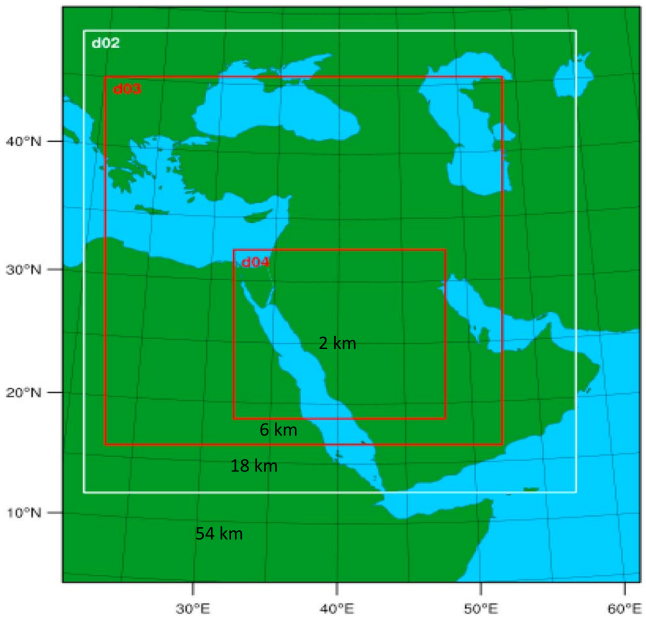

Figure 8. WRF domain configuration for the Saudi dust storm case (Pokharel, 2016). do1, do2, do3, and do4 represent domains of 54, 18, 6, and 2 km resolution, respectively.

deepening of the cold, negatively tilted trough, as falling heights revealed the deepening upper air disturbance over the Middle East and northwestern parts of Saudi Arabia, such as Tabuk, Al Jawf, Sakakah, and Ha'il.

3.2.2. WRF Simulation Analyses

In the afternoon (at 1500 UTC) of 8 March 2009 there was a well-mixed convective boundary layer upstream of the Sarawat Mountain, inferred from the WRF-simulated 18 km grid spacing model data of temperature and wind speed at 850 and 925 hPa (Figures 8 and 9). At 0000 UTC of 9 March, the air adjacent to the bottom of the lee slope of the eastern edge of the Sarawat Mountains was warmer, indicative of the preceding downslope wind and thereby advection of the residual well-mixed boundary layer from the previous afternoon, which had formed above the Sarawat Mountains. This is very similar to the Harmattan case discussed in section 3.1.2. The presence of the EML is consistent with the observed soundings (Figures 6a and 6b). Also, the deep dry adiabatic lapse rate of the early morning hours on 9 March from the sounding at Ha'il and Al-Madinah is represented by the structure of the isentropes in the WRF simulation in Figure 10a.

In order to verify the downslope winds from the soundings at Ha'il and Al-Madinah, we again analyzed vertical cross sections of the isentropic surfaces of the WRF-simulated data sets (18 km grid spacing) across the mountain range, here a west-east cross section of the Sarawat Mountains near the sounding stations (Figure 10a). At 0600 UTC on 9 March, there was upstream blocking of the prevailing westerly winds, shown by the bulging of isentropic surfaces at upper levels at the northwestern edge of the Sarawat Mountains (at 26.7°N, 37°E; Figure 10a). The presence of the blocking condition of the prevailing wind is also seen by the low upstream Froude number, Fr = 0.42 at 0600 UTC, indicative of the lack of the sufficient kinetic energy of the prevailing wind to cross the mountains at that time. Later, the kinetic energy of the prevailing wind increased as shown by the increased magnitude of Froude number, which was 0.93 at 0900 UTC (Figure 10b) and more (~1) afterward (e.g., subcritical to supercritical flow) at the aforesaid location, where the air subsequently accelerated as a downslope wind in the lee of the Sarawat Mountains. The flow of the downslope wind is also inferred by the sinking of the isentropic surfaces sharply in the lee of the mountains (Figure 10b). The cross-mountain flow is associated with the gradient of

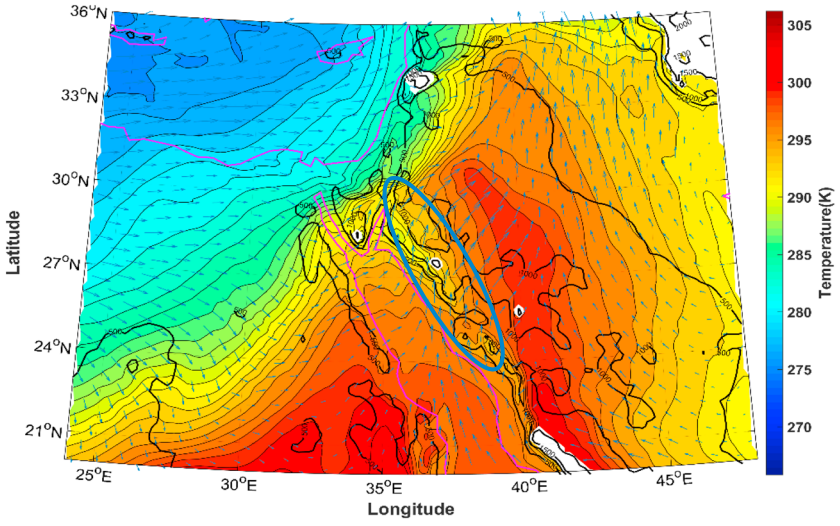

Figure 9. Temperature and wind speed/direction at 850 hPa at 1500 UTC on 8 March 2009 (18 km resolution). The blue circled area marks warming area of the windward side of the Sarawat Mountains in the afternoon of 8 March 2009. The black contours mark the orographic height in step of 500 m.

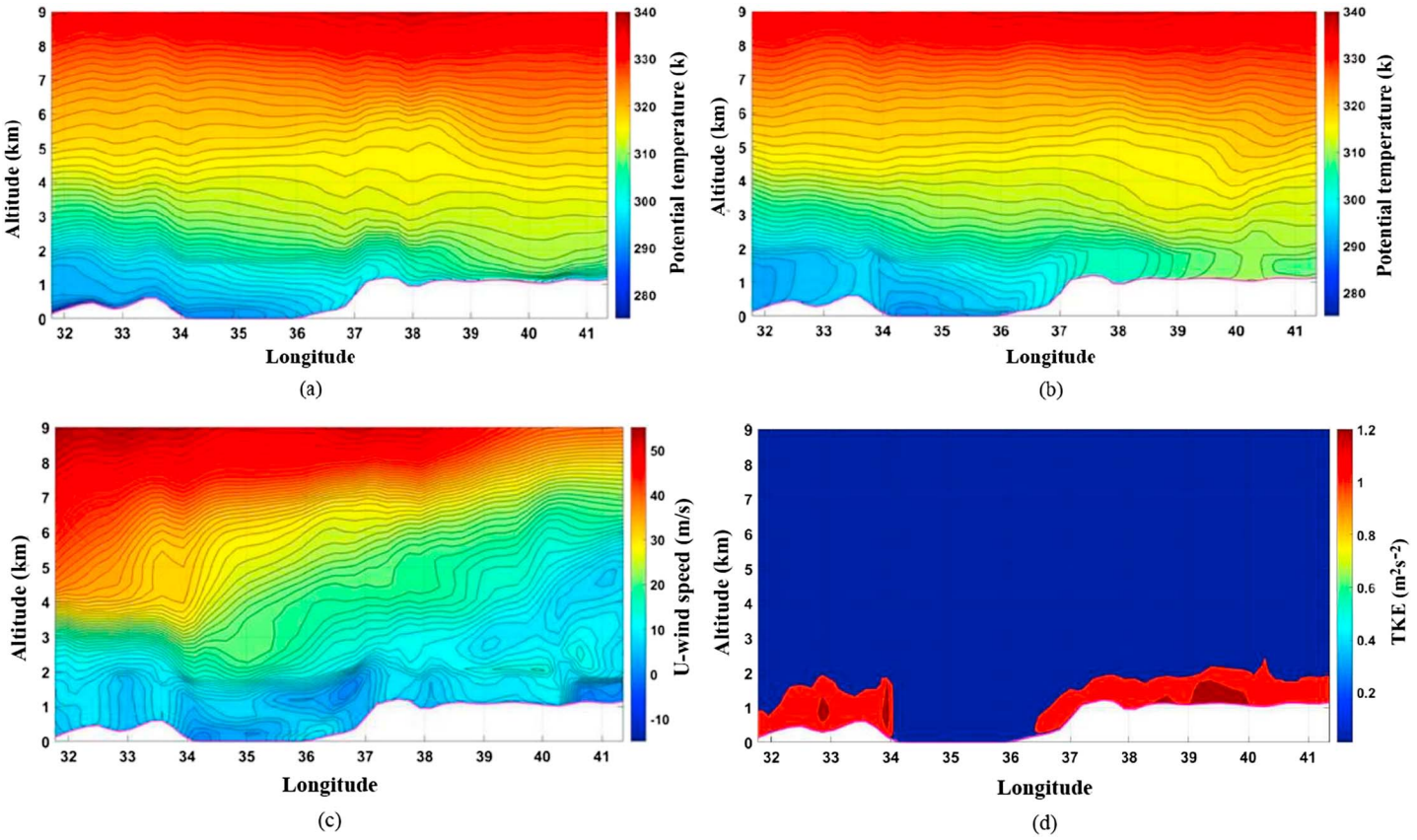

Figure 10. (a) Vertical cross sections of potential temperature (shaded) at 26.7°N at 0600 UTC 9 March 2009 (18 km resolution WRF product). (b) Vertical cross sections of potential temperature (shaded) at 26.7°N at 0900 UTC 9 March 2009 (18 km resolution WRF product). (c) Vertical cross sections of *u*-wind components (shaded) at 26.7°N at 0900 UTC 9 March 2009 (18 km resolution WRF product). Positive and negative *u*-wind components indicate westerly and easterly winds, respectively. (d) Vertical cross sections of TKE at 26.7°N at 0900 UTC 9 March 2009 (18 km resolution WRF product).

the pressure between the windward and leeward side of the Sarawat Mountains that accelerated the air toward the pressure minimum well below the upper level wave disturbance in the narrow layer between the Sarawat Mountains and the midlevel inversion. The downslope air advection is consistent with the horizontal veering direction of the wind during the dust storms recorded in the previously mentioned surface stations during that time period. When this strong downslope wind and its accompanying strong low-level vertical wind shear interacted with the buoyant warm air in the lee of the mountains, turbulent eddies developed (Figures 10c and 10d) and lead to a well-mixed boundary layer favorable for dust emission. Indeed, dust storms were observed at stations on the lee of the Sarawat Mountains, by the observations in Weather Underground at the time of the hydraulic jump. The co-occurrence of the hydraulic jump, the associated increase in turbulent mixing and near-surface peak winds, and the associated dust emission and uplift in this case is very similar to the case in northwest Africa described earlier. The different geographical locations of these downslope winds suggest that associated dust emission might be relatively common, but their climatological importance is not well understood.

3.3. Bodélé Depression Dust Storm Case Study

3.3.1. Joint Observational and Model Analyses

Due to the unavailability of the soundings in and around Chad at the time of the early period of 8 December 2011, we could not analyze the rawinsonde data for this case study. Though there were some observational stations in Chad, only one station, which is Ndjamena (12.13°N, 15°E) (southeast from the Bodélé Depression) (Figure 11), recorded dust storms with a northeasterly wind of 3 m/s speed at 0600 UTC on 8 December 2011 and the visibility was recorded as 6 km at that time. Given the weak wind speed that is well below typical threshold winds for dust emission, the record likely reflects dust in suspension that has been emitted upstream toward the center of the Bodélé Depression (Figure 12).

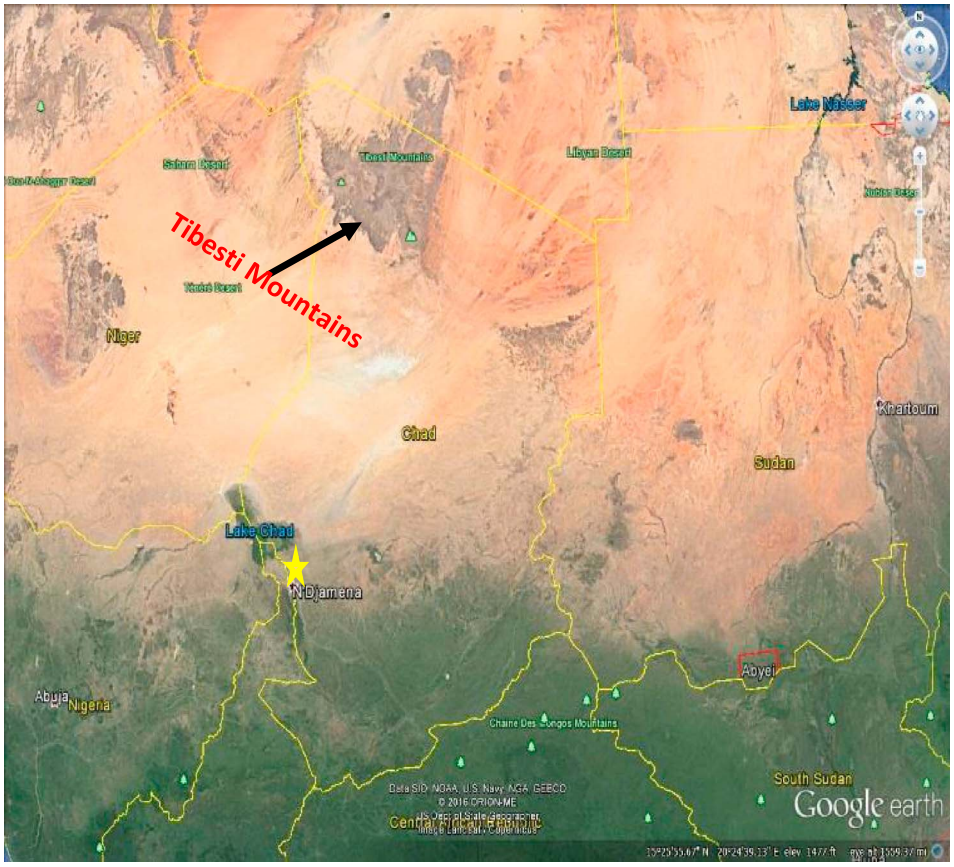

Figure 11. The surface observational station, which is shown by a yellow star, at Ndjamena in Chad where the occurrence of dust storm at 0600 UTC on 8 December 2011 was recorded (source: wunderground.com).

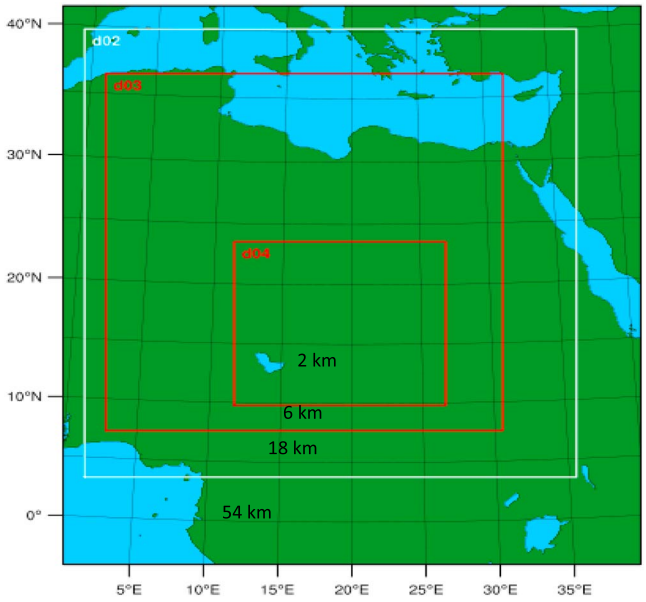

Figure 12. WRF domain configuration for the Bodélé Depression dust storm case (Pokharel, 2016). do1, do2, do3, and do4 represent domains of 54, 18, 6, and 2 km resolution, respectively.

At 0600 UTC on 8 December 2011, NAAPS shows the first evolution of the dust in the regions west/southwestward and equatorward of the Tibesti Mountains with 2560 μg/m^3 of surface dust concentration. By midday the strength has increased by almost a factor of 4 (10,240 μg/m^3) and the areal extension of the dust substantially increased in the southwest of the Tibesti Mountains. Similarly, MERRA-2 shows that the dust-scattering AOT was 0.12 at 0600 UTC in the west/southwestward of the Tibesti and by midday it reached up to 0.27 over that region.

The analysis of the midtropospheric wind flow observed from the MERRA data set is to a large degree similar to the one over northwest Africa. There was the development of a positively tilted trough accompanying ageostrophic wind consistent with the concentration of a cyclonic vorticity maximum near the trough axis at 19–20°N, 17–19°E at 0600 UTC 8 December. The positively tilted trough strengthened slightly until the occurrence of the dust storm. Though the strength of the positively tilted trough was weak, falling heights still indicate the upper air disturbance over the northeast of Niger, north and northwestern regions of Chad, which included Aozou, and the region southeast of Libya.

3.3.2. WRF Simulation Analyses

To analyze the presence of the downslope wind during the early periods of 8 December, the higher-resolution data sets of 6 km grid

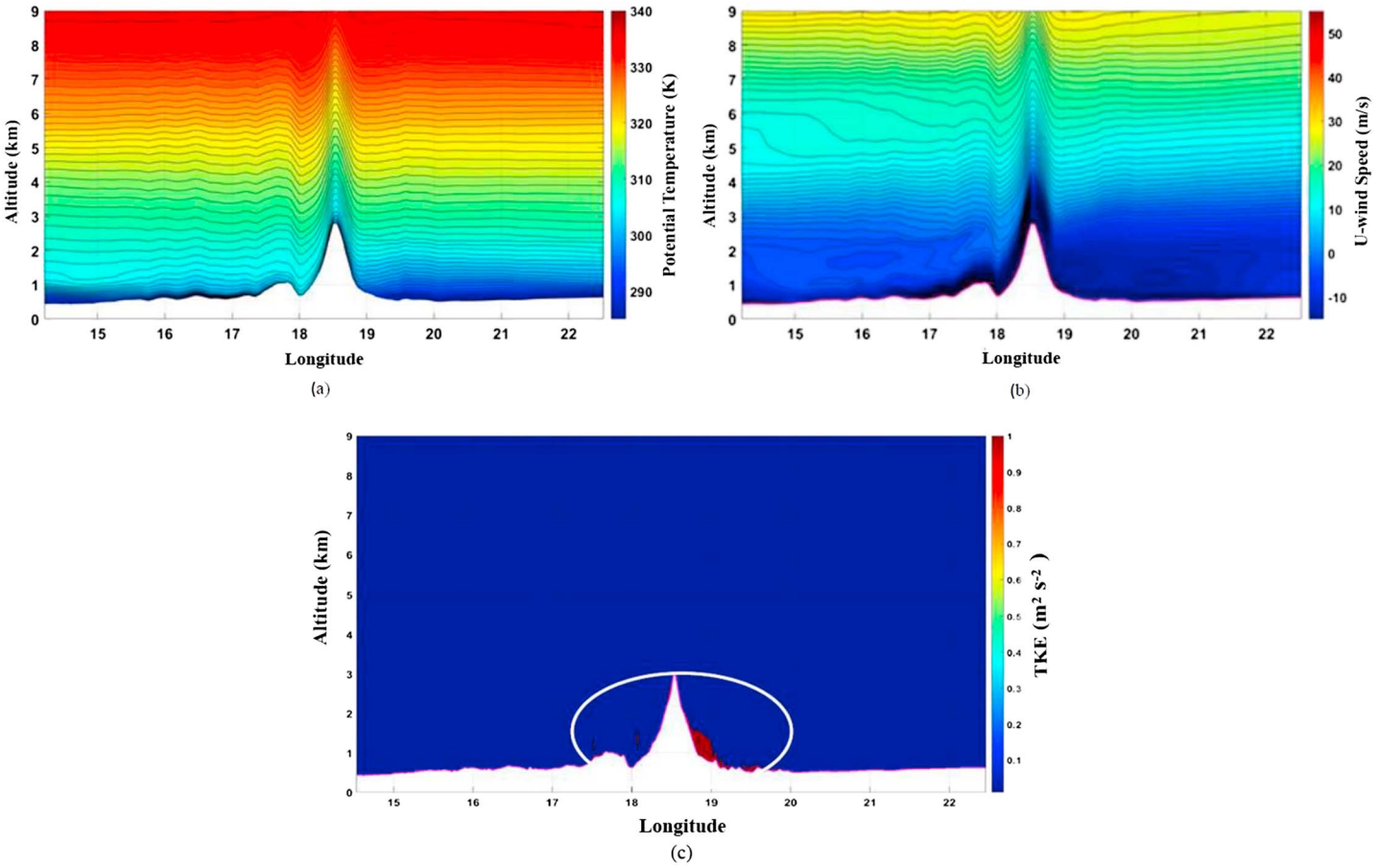

Figure 13. (a) Vertical cross sections of potential temperature (shaded) at 19.78°N at 0000 UTC on 8 December 2011 (6 km resolution WRF product). (b) Vertical cross sections of *u*-wind speed (shaded) at 19.78°N at 0000 UTC on 8 December 2011 (6 km resolution WRF product). Positive and negative *u*-wind components indicate westerly and easterly winds, respectively. (c) Vertical cross sections of turbulence kinetic energy (TKE) at 19.78°N at 0700 UTC on 8 December 2011 (2 km resolution WRF product). The white circled area marks the TKE.

spacing of the WRF simulation were used to plot the vertical cross sections of isentropic surfaces (Figure 13a). Figure 13a shows that there were bulging isentropic surfaces above the Tibesti Mountains at 0000 UTC over the 19.78°N, 18.0–18.5°E region (cross sections across east-west axis) and the perturbation of the *u*-wind speed components (6 km grid spacing) at that location. Similarly, at that location, the Froude number as defined in equation (1) was 0.2, which indicates the blocking of the prevailing winds at that time due to the insufficient kinetic energy of the air parcels to cross the mountains. Over time (i.e., 0600 UTC and afterward) the sinking of the isentropic surfaces were significant at that location, indicative of the flow of the downslope wind (dominance of kinetic energy over the potential energy of the air parcels) in the lee of the mountains—for example, transition from subcritical to supercritical flow. This is consistent with the direction of the northeasterly wind flow during the occurrence of the dust storm at that time. When this downslope wind interacted with the warm buoyant air column present in the region southwestward/south of the mountains (Figures 13b and 13c) there was emission of the diatomite dust caused by the generation of the significant amount of turbulent eddies. This turbulence was the result of the summation of the strong wind shear and the buoyancy at that time as given in the TKE tendency (equation (2)). This is consistent with the dust storm observed by Weather Underground at Ndjamena at 0600 UTC on 8 December 2011.

4. Conclusions

We find that in the early stages of three severe dust storms downslope winds developed, resulting from a transition from a subcritical to supercritical flow in the lee of three heterogeneously oriented mountain ranges in North Africa and the Arabian Peninsula. These downslope winds resulted in strong low-level vertical

wind shear, interacted with the development of near-surface positive buoyant air during the morning, and generated significant TKE as a result of boundary layer mixing accompanying both kinematically and thermodynamically driven buoyancy. This TKE led to a well-mixed/turbulent surface layer circulations causing moderate meso-γ- to β-scale dust storms at the early stage of later severe dust storms affecting large areas. These precursor dust storms likely ablated dust and suspended it, preconditioning the lower atmosphere for the larger-scale and more prolonged dust storm events to follow.

While previous work had identified a hydraulic jump as a signal of downslope wind storm genesis in a case study of northwest Africa (Gläser, Knippertz, & Heinold, 2012), we show here that such events are also found in other, quite different locations when similar synoptic-scale flows interact with mountain ranges. We find evidence for a simulated hydraulic jump in the Bodélé Depression, where substantial dust emission has been attributed to the formation of nocturnal low-level jets, downslope winds, and gap winds (e.g., Fiedler et al., 2013; Schepanski et al., 2009; Washington & Todd, 2005) and on the Arabian Peninsula in an event that occurred outside of the dominant dust storm season and has not been analyzed in depth before. The high-resolution modeling in the present work indicates that favorable conditions for leeside TKE generation play an important role in generating the dust-emitting peak winds during the early stages of such events. Turbulence kinetic energy maxima cannot be resolved by coarse-resolution data; therefore, dust emission associated with leeside hydraulic jumps would be missed. This reveals that if we simulate higher-resolution data sets, we can see clear signals of conditions favorable for turbulent eddies responsible for creating well-mixed layers in the atmosphere to deflate the dust from the surface. Our case studies suggest that the synoptic situation gives a clear indication for the precursor signals, indicating that the occurrence of such events and associated peak winds could be predicted by a state-of-the-science numerical model. Further, we see that high-resolution modeling studies are needed to understand the relative contribution of downslope wind-driven dust emission to the total dust budget. Such estimates would help to assess the impact of the lack of this mechanism in coarse-resolution models and potentially develop a way for correcting it.

Acknowledgments

We would like to thank K.C. King, Robert David, Stephen Noble, Farnaz Hosseinpour, and Kacie Shourd for their help in collecting the observational data sets and running the WRF model. We would also like to thank the National Science Foundation (NSF) and National Center for Atmospheric Research (NCAR) for providing the computational support. We would also like to thank to reviewers and the Editor Minghua Zhang for their insightful comments and suggestions. This work is not funded by any government or private agency. The Division of Atmospheric Sciences of the Desert Research Institute under the direction of Marc Pitchford funded the publication of this research. We would like to state that data used here from the external sources are from cited references. The authors declare that there are no conflicts of interest.

References

Alharbi, B. H., Maghrabi, A., & Tapper, N. (2013). The March 2009 dust event in Saudi Arabia-Precursor and Supportive Environment. *Bulletin of the American Meteorological Society*, *94*, 515–528. https://doi.org/10.1175/bams-d-11- 00118.1

Barkan, J., Kutiel, H., & Alpert, P. (2004). Climatology of dust sources in North Africa and the Arabian Peninsula, based on TOMS data. *Indoor and Built Environment*, *13*, 407–419. https://doi.org/10.1177/1420326x04046935

Betts, A. K. (1986). A new convective adjustment scheme.1. Observational and theoretical basis. *Quarterly Journal of the Royal Meteorological Society*, *112*, 677–691. https://doi.org/10.1256/smsqj.47306

Betts, A. K., & Miller, M. J. (1986). A new convective adjustment scheme. 2 Single column tests using Gate wave, Bomex, Atex, and Arctic air-mass data sets. *Quarterly Journal of the Royal Meteorological Society*, *112*, 693–709. https://doi.org/10.1002/qj.49711247308

Burton, R. R., Devine, G. M., Parker, D. J., Chazette, P., Dixon, N., Flamant, C., & Haywood, J. M. (2013). The Harmattan over West Africa: Nocturnal structure and frontogenesis. *Quarterly Journal of the Royal Meteorological Society*, *139*, 1364–1373. https://doi.org/10.1002/qj.2036

Chen, F., & Dudhia, J. (2001). Coupling an advanced land surface-hydrology model with the Penn State-NCAR MM5 modeling system. Part I: Model implementation and sensitivity. *Monthly Weather Review*, *129*, 569–585. https://doi.org/10.1175/1520-0493(2001)129<0569:caalsh>2.0.co;2

Dudhia, J. (1989). Numerical study of convection observed during the winter monsoon experiment using a mesoscale two dimensional model. *Journal of the Atmospheric Sciences*, *46*, 3077–3107. https://doi.org/10.1175/1520-0469(1989)046<3077:nsocod>2.0.co;2

Durran, D. R. (1990). Mountain waves and downslope winds. In W. Blumen (Eds.), *Atmospheric Processes over Complex Terrain*. *Meteorological Monographs* (Vol. 23), Boston, MA: American Meteorological Society. https://doi.org/10.1007/978-1-935704-25-6_4

Ek, M. B., Mitchell, K. E., Lin, Y., Rogers, E., Grunmann, P., Koren, V., … Tarpley, J. D. (2003). Implementation of Noah land surface model advances in the National Centers for Environmental Prediction operational mesoscale Eta model. *Journal of Geophysical Research: Atmospheres*, *108*(D22), 8851. https://doi.org/10.1029/2002JD003296

Fiedler, S., Kaplan, M. L., & Knippertz, P. (2015). Supporting information for the importance of Harmattan surges for the emission of North African dust aerosol. *Geophysical Research Letters*, *42*, 9495–9504. https://doi.org/10.1002/2015GL065925

Fiedler, S., Schepanski, K., Heinold, B., Knippertz, P., & Tegen, I. (2013). Climatology of nocturnal low-level jets over North Africa and implications for modeling mineral dust emission. *Journal of Geophysical Research: Atmospheres*, *118*, 6100–6121. https://doi.org/10.1002/jgrd.50394

Gläser, G., Knippertz, P., & Heinold, B. (2012). Orographic effects and evaporative cooling along a subtropical cold front: The case of the spectacular Saharan dust outbreak of March 2004. *Monthly Weather Review*, *140*, 2520–2533. https://doi.org/10.1175/MWR-D-11-00315.1

Heinold, B., Knippertz, P., Marsham, J. H., Fiedler, S., Dixon, N. S., Schepanski, K., … Tegen, I. (2013). The role of deep convection and nocturnal low-level jets for dust emission in summertime West Africa: Estimates from convection permitting simulations. *Journal of Geophysical Research: Atmospheres*, *118*, 4385–4400. https://doi.org/10.1002/jgrd.50402

Houghton, D. D., & Kashara, A. (1968). Nonlinear shallow fluid flow over an isolated ridge. *Communications on Pure and Applied Mathematics*, *21*, 1–23.

Janjić, Z. I. (1994). The step-mountain Eta coordinate model—further developments of the convection, viscous sub-layer, and turbulence closure schemes. *Monthly Weather Review*, *122*, 927–945. https://doi.org/10.1175/1520-0493(1994)122<0927:tsmecm>2.0.co;2

Janjić, Z. I. (1996). The surface layer in the NCEP Eta model, Preprints. In *11th Conference on Numerical Weather Prediction* (pp. 354–355). Am. Norfolk,Va: American Meteorological Society.
Janjić, Z. I. (2001). Nonsingular implementation of the Mellor-Yamada level 2.5 scheme in the NCEP Meso model, Off. Note 437, 61 pp.
Kalu, A. E. (1979). The African dust plume: Its characteristics and propagation across West Africa in winter. In C. Morales (Ed.), *Saharan Dust: Mobilization, Transport and Deposition* (pp. 95–118). Chichester, UK: John Wiley and Sons.
Klemp, J. B., & Lilly, D. K. (1975). The dynamics of wave induced downslope winds. *Journal of the Atmospheric Sciences*, *32*, 320–339.
Klose, M., & Shao, Y. (2013). Large-eddy simulation of turbulent dust emission. *Aeolian Research*, *8*, 49–58.
Koren, I., & Kaufman, Y. J. (2004). Direct wind measurements of Saharan dust events from Terra and Aqua satellites. *Geophysical Research Letters*, *31*, L06122. https://doi.org/10.1029/2003GL019338
Koren, I., Kaufman, Y. J., Washington, R., Todd, M. C., Rudich, Y., Martins, J. V., & Rosenfeld, D. (2006). The Bodélé Depression: A single spot in the Sahara that provides most of the mineral dust to the Amazon forest. *Environmental Research Letters*, *1*, 014005.
Maghrabi, A., Alharbi, B., & Tapper, N. (2011). Impact of the March 2009 dust event in Saudi Arabia on aerosol optical properties, meteorological parameters, sky temperature and emissivity. *Atmospheric Environment*, *45* (13), 2164–2173, https://doi:10.1016/j.atmosenv.2011.01.071
Mellor, G. L., & Yamada, T. (1974). A hierarchy of turbulence closure models for planetary boundary layers. *Journal of the Atmospheric Science*, *31*, 1791–1806. https://doi.org/10.1175/1520-0469(1974)031<1791:AHOTCM>2.0.CO;2
Mlawer, E. J., Taubman, S. J., Brown, P. D., Iacono, M. J., & Clough, S. A. (1997). Radiative transfer for inhomogeneous atmospheres: RRTM, a validated correlated-*k* model for the longwave. *Journal of Geophysical Research: Atmospheres*, *102*, 16,663–16,682. https://doi.org/10.1029/97JD00237
New, M. G., Lister, D., Hulme, M., & Makin, I. (2002). A high-resolution data set of surface climate for terrestrial land areas. *Climate Research*, *21*, 1–25.
Ozer, P. (2001). Les lithometeores en region sahelienne. *International Journal of Geo-Eco-Tropical*, *24*, 1–317.
Peltier, W. R., & Clark, T. L. (1979). The evolution and stability of finite-amplitude mountain waves. Part II: Surface wave drag and severe downslope winds. *Journal of the Atmospheric Sciences*, *36*, 1498–1529.
Pokharel, A. K. (2016). Atmospheric dynamics of sub-tropical dust storms, University of Nevada, Reno, ProQuest Dissertations Publishing, 2016. 10161308. Retrieved from: https://search.proquest.com/openview/da62a119163cda173814073c75d3bc4e/1?pq-origsite=gscholar&cbl=18750&diss=y
Pokharel, A. K., Kaplan, M. L., & Fiedler, S. (2016). Atmospheric dynamics of the Harmattan surge on March 2, 2004. *ProScience*, *3*, 84–93. https://doi.org/10.14644/dust.2016.014
Prospero, J. M., Ginoux, P., Torres, O., Nicholson, S. E., & Gill, T. E. (2002). Environmental characterization of global sources of atmospheric soil dust identified with the Nimbus 7 Total Ozone Mapping Spectrometer (TOMS) absorbing aerosol product. *Reviews of Geophysics*, *40*(1), 1002. https://doi:10.1029/2000RG000095
Rinecker, M. M., Suarez, M. J., Gelaro, R., Todling, R., Bacmeister, J., Liu, E., … Woollen, J. (2011). MERRA: NASA's Modern-Era Retrospective Analysis for Research and Applications. *Journal of Climate*, *24*, 3624–2648. https://doi.org/10.1175/JCLI-D-11-00015.1
Rubin, J. I., Reid, J. S., Hansen, J. A., Anderson, J. L., Collins, N., Hoar, T. J., … Zhang, J. (2016). Development of the Ensemble Navy Aerosol Analysis Prediction System (ENAAPS) and its application of the Data Assimilation Research Testbed (DART) in support of aerosol forecasting. *Atmospheric Chemistry and Physics*, *16*, 3927–3951. https://doi.org/10.5194/acp-16-3927-2016
Schepanski, K., Tegen, I., Todd, M. C., Heinold, B., Bönisch, G., Laurent, B., & Macke, A. (2009). Meteorological processes forcing Saharan dust emission inferred from MSG-SEVIRI observations of subdaily dust source activation and numerical models. *Journal of Geophysical Research*, *114*, D10201. https://doi.org/10.1029/2008JD010325
Skamarock, W. C., J. B. Klemp, J. Dudhia, D. O. Gill, D. M. Barker, M. G. Duda, X.-Y. Huang, W. Wang, and J. G. Powers (2008). A description of the Advanced Research WRF version 3, NCAR/TN- 475+STR, 113 pp.
Smith, R. B. (1985). On severe downslope winds. *Journal of Atmospheric Science*, *42*, 2597–2603.
Smolarkiewicz, P., & Rotunno, R. (1989). Low Froude number flow past three- dimensional obstacles. Part 1: Baroclinically generated lee vortices. *Journal of Atmospheric Science*, *46*, 1154–1164.
Stull, R. (2000). Meteorology for Scientists and Engineers. Pacific Grove/Brooks Cole.
Thompson, G., Field, P. R., Hall, W. D., & Rasmussen, R. M. (2006). A new bulk microphysics parameterization for WRF and MM5, Seventh Weather and Research Forecasting Workshop, Boulder, Co: NCAR, National Center for Atmospheric Research.
Thompson, G., Rasmussen, R. M., & Manning, K. (2004). Explicit forecasts of winter precipitation using an improved bulk microphysics scheme. Part I: Description and sensitivity analysis. *Monthly Weather Review*, *132*, 519–542. https://doi.org/10.1175/1520- 0493(2004)132<0519:efowpu>2.0.co;2
Todd, M. C., Washington, R., Martins, J. V., Dubovik, O., Lizcano, G., M'Bainayel, S., & Engelstaedtler, S. (2007). Mineral dust emission from the Bodélé Depression, northern Chad, during BoDEx 2005. *Journal of Geophysical Research Atmosphere*, *12*, D06207. https://doi:10.1029/2006JD007170
Washington, R., & Todd, M. C. (2005). Atmospheric controls on mineral dust emission from the Bodélé Depression, Chad: The role of the low level jet. *Geophysical Research Letters*, *32*, L17701. https://doi.org/10.1029/2005GL023597
Washington, R., Todd, M., Middleton, N. J., & Goudie, A. S. (2003). Dust storm source areas determined by the Total Ozone Monitoring Spectrometer and surface observations. *Annals of the Association of American Geographers*, *93*, 297–313. https://doi.org/10.1111/1467-8306.9302003